Cellular/Molecular

Evolution Increases Primates Brain Complexity Extending RbFOX1 Splicing Activity to LSD1 Modulation

Chiara Forastieri,[1] Maria Italia,[1] Emanuela Toffolo,[1] Elena Romito,[1] Maria Paola Bonasoni,[2] Valeria Ranzani,[3] Beatrice Bodega,[3,4] Francesco Rusconi,[1] and Elena Battaglioli[1]

[1]Department of Medical Biotechnology and Translational Medicine, Università degli Studi di Milano, Segrate, 20090, Italy, [2]ASMN Santa Maria Nuova, Reggio Emilia, 42123, Italy, [3]Istituto Nazionale di Genetica Molecolare "Romeo ed Enrica Invernizzi," Milano, 20122, Italy, and [4]Department of Biosciences, Università degli Studi di Milano, Milano, 20133, Italy

Recent branching (100 MYA) of the mammalian evolutionary tree has enhanced brain complexity and functions at the putative cost of increased emotional circuitry vulnerability. Thus, to better understand psychopathology, a burden for the modern society, novel approaches should exploit evolutionary aspects of psychiatric-relevant molecular pathways. A handful of genes is nowadays tightly associated to psychiatric disorders. Among them, neuronal-enriched RbFOX1 modifies the activity of synaptic regulators in response to neuronal activity, keeping excitability within healthy domains. We here dissect a higher primates-restricted interaction between RbFOX1 and the transcriptional corepressor Lysine Specific Demethylase 1 (LSD1/KDM1A). A single nucleotide variation (AA to AG) in *LSD1* gene appeared in higher primates and humans, endowing RbFOX1 with the ability to promote the alternative usage of a novel 3′ AG splice site, which extends LSD1 exon E9 in the upstream intron (E9-long). Exon E9-long regulates LSD1 levels by Nonsense-Mediated mRNA Decay. As reintroduction of the archaic *LSD1* variant (AA) abolishes E9-long splicing, the novel 3′ AG splice site is necessary for RbFOX1 to control LSD1 levels. LSD1 is a homeostatic immediate early genes (IEGs) regulator playing a relevant part in environmental stress-response. In primates and humans, inclusion of LSD1 as RbFOX1 target provides RbFOX1 with the additional ability to regulate the IEGs. These data, together with extensive RbFOX1 involvement in psychiatric disorders and its stress-dependent regulation in male mice, suggest the RbFOX1-LSD1-IEGs axis as an evolutionary recent psychiatric-relevant pathway. Notably, outside the nervous system, RbFOX2-dependent LSD1 modulation could be a candidate deregulated mechanism in cancer.

Key words: **evolution; lysine specific demethylase 1; major depressive disorder; non-sense-mediated decay; psychiatric disorders; RNA-binding Fox homolog 1**

Significance Statement

To be better understood, anxiety and depression need large human genetics studies aimed at further resolving the often ambiguous, aberrant neuronal pathomechanisms that impact corticolimbic circuitry physiology. Several genetic associations of the alternative splicing regulator RbFOX1 with psychiatric conditions suggest homeostatic unbalance as a neuronal signature of psychopathology. Here we move a step forward, characterizing a disease-relevant higher primates-specific pathway by which RbFOX1 acquires the ability to regulate neuronal levels of Lysine Specific Demethylase 1, an epigenetic modulator of environmental stress response. Thus, two brain-enriched enzymes, independently shown to homeostatically protect neurons with a clear readout in terms of emotional behavior in lower mammals, establish in higher primates and humans a new functional cooperation enhancing the complexity of environmental adaptation and stress vulnerability.

Received Sep. 2, 2021; revised Feb. 28, 2022; accepted Mar. 3, 2022.

Author contributions: C.F., F.R., and E.B. designed research; C.F., M.I., E.T., E.R., M.P.B., and V.R. performed research; C.F., M.I., E.T., B.B., F.R., and E.B. analyzed data; C.F., F.R., and E.B. edited the paper; M.P.B. contributed unpublished reagents/analytic tools; F.R. and E.B. wrote the first draft of the paper; F.R. and E.B. wrote the paper.

This work was supported by CARIPLO Foundation Grant 2016-0908 and KAUST CRG 2018 to E.B. and PSR_2019 to F.R. We thank Leda Paganini for the initial contribution to the work; Graziano Rocchi for providing nonprimates and primate cell lines; and Marco Venturin for postmortem human cerebellar and hippocampal samples.

The authors declare no competing financial interests.

Correspondence should be addressed to Elena Battaglioli at elena.battaglioli@unimi.it or Francesco Rusconi at francesco.rusconi@unimi.it.

https://doi.org/10.1523/JNEUROSCI.1782-21.2022

Introduction

Splicing modulation represents one of the most important sources of proteome complexity, especially in the mammalian brain, where it is spatially and temporally modulated. Within neurons, peculiar splicing pathways also respond to electrical activity contributing to balancing the input/output ratio (Eom et al., 2013; Longaretti et al., 2020b; Thalhammer et al., 2020), thus modulating the availability of synaptic, but also nuclear, factors. Such mechanisms have been gathered as homeostatic splicing and guarantee efficient information processing in the frame of

excitatory circuitry preservation (Turrigiano, 2012). Alterations of this process can profoundly impact in normal brain physiology, causing different neurologic pathologies, from epileptic to neurodevelopmental and neuropsychiatric disorders (Gehman et al., 2011; Quesnel-Vallières et al., 2016; Thalhammer et al., 2020).

Homeostatic splicing has been described thanks to the independent characterization of few RNA binding proteins highly enriched in neurons, including RbFOX1/A2BP1 (Lee et al., 2009; Gehman et al., 2011), nSR100/SRRM4 (Irimia et al., 2014; Quesnel-Vallières et al., 2016), NOVA1/2 (Zhang et al., 2010; Eom et al., 2013), and SAM68 (Iijima et al., 2011). All these factors undergo neuronal activity-dependent modulation allowing a timely program of splicing regulation devoted to synaptic-related and neuronal connectivity-instrumental targets (Lee et al., 2009; Gehman et al., 2011; Eom et al., 2013; Quesnel-Vallières et al., 2016). Indeed, homeostatic splicing reduces neuronal excitability within a homeostasis-demanding window that follows neuronal depolarization (Thalhammer et al., 2020). Consistently with RbFOX1 splicing activity, which is aimed at reestablishing resting-like splicing pattern via attenuation of neuronal excitability, *RbFOX1*^{KO} mice are hyperexcitable (Gehman et al., 2011). One of the prominent neuronal RbFOX1 mRNA targets is the glutamate ionotropic NMDAR constitutive subunit GluN1. Interestingly, RbFOX1 regulates exon 5 inclusion (Lee et al., 2009) with the purpose to limit NMDAR activity, negatively impacting neuroplasticity modification and memory formation with homeostatic purposes (Sengar et al., 2019). In accordance with this role, mutations in RbFOX1 have been associated with multiple neurologic, neurodegenerative, and neuropsychiatric disorders, including epilepsy (Lal et al., 2015), schizophrenia (Xu et al., 2008), aggressive behavior (Fernàndez-Castillo et al., 2020), autism (Lee et al., 2016), and attention deficit and hyperactivity disorder (Elia et al., 2010). Recently, an important genome-wide association study listed *RbFOX1* as one of the genes mostly associated with human depression, a pathology that holds important environmental stress-related determinants (Sullivan, 2015), along with overload of homeostatic mechanisms.

In this work, we identified a novel RbFOX1 target gene, namely *Lysine Specific Demethylase 1* (*LSD1*) that might help deciphering recently identified implications of RbFOX1 in psychiatric conditions. LSD1 is a transcriptional restrainer of neuroplastic gene expression belonging to the CoREST/HDAC2 corepressor complex (Guan et al., 2009; Wang et al., 2015; Rusconi et al., 2017). In the brain, LSD1 activity is modulated by neuroLSD1, a dominant negative neurospecific splicing isoform generated by splicing inclusion of exon E8a. The relative ratio between LSD1 and neuroLSD1 sets LSD1 repressive activity and, as a result, target genes expression. The LSD1/neuroLSD1 ratio is developmentally regulated during synaptogenesis and aging through the concerted activity of its master splicing modulator nSR100/SRRM4 and the ancillary splicing factor NOVA1 (Rusconi et al., 2015). Remarkably, the LSD1/neuroLSD1 ratio can also be modulated in response to environmental stress, a process that is likely controlled by the same splicing factors, nSR100/SRRM4 and NOVA1 (Rusconi et al., 2016; Longaretti et al., 2020b). In particular, we showed that activity-induced splicing modulation causes a transient shift of LSD1/neuroLSD1 ratio in favor of LSD1 that is instrumental to negative feedback, ultimately reducing glutamatergic synaptic excitability (Rusconi and Battaglioli, 2018; Longaretti et al., 2020b; Rusconi et al., 2020). Transient increase of LSD1 activity fosters repression of a transcriptional pathway controlling the immediate early genes (IEGs) and two negative regulators of the endocannabinoid system, MAGL and ABHD6 (Longaretti et al., 2020a). Activation of this pathway is dependent on glutamate via NMDAR activation that is required to induce exon E8a skipping (Longaretti et al., 2020b). Thus, the fine-tuning of LSD1/neuroLSD1 ratio can be rightfully listed as a homeostatic splicing. All this evidence suggests that both RbFOX1 and LSD1 are independently involved in neuronal homeostasis.

We here show that, only in humans and higher primates, these two pathways converge, providing LSD1 with a specific RbFOX1 regulation. Indeed, a single nucleotide variation only present in higher primates' *LSD1* gene, creates a cryptic splicing acceptor AG dinucleotide within INT8a-9, regulated by RbFOX1. The alternative usage of such AG site extends exon E9 and generates the alternative LSD1 exon E9-long. E9-long includes a premature STOP codon, which, by non-sense-mediated decay (NMD) reduces LSD1 levels. With this work, we provide a novel higher primate's restricted RbFOX1-dependent regulation of LSD1 levels potentially important to better define RbFOX1 and LSD1 roles in psychopathology.

Materials and Methods

Cell cultures. Cell lines used are as follows: human neuroblastoma cell lines SH-SY5Y (Sigma Aldrich, ECACC) and SK-N-BE (ATCC), human ovarian granulosa tumor cell line COV434 (Sigma Aldrich, ECACC), and mouse neuroblastoma cell line Neuro2A (Sigma Aldrich, ECACC). EFU1 fibroblast cell lines derived from *Eulemur fulvus*, LCA1 from *Lemur catta*, and MMU *Macaca mulatta* (MMU) lymphoblast cell line were a generous gift from Graziano Rocchi. All cell lines were cultured according to standard procedures. SH-SY5Y-TetON derived clones were cultured in complete medium added with antibiotics (G418 400 μg/ml alone or with hygromycin B 100 μg/ml).

NMD. NMD was inhibited by cycloheximide (CHX) treatment at a concentration of 100 μg/ml for 6 and/or 8 h as in (Cardamone et al., 2017).

Cell lines transfection and vectors. Cells were transfected using Lipofectamine LTX and PLUS Reagent (15338, Invitrogen) according to the manufacturer's protocol. SH-SY5Y cells were transfected with human minigene MG2700 (hMG2700) carrying 2700 bp human genomic fragment, including exon E8a flanking intronic region (chr1:23 065,790-23 068,538) cloned in the NdeI restriction site of pBS-Splicing; lemurMG2700 containing the corresponding genomic fragment obtained through high-fidelity PCR from LCA1 cells gDNA; hMG2700 archaic MUT [AA] and lemurMG2700 MUT [AG] obtained by conventional site-directed mutagenesis using specific primers. The indicated genomic coordinate refers to human genome assembly GRCh38/hg38. Other expression plasmids used are as follows: pCDNA3.1-Flag-nSR100, containing human full-length nSR100 cDNA cloned into pCDNA3.1 (V79020, Invitrogen) from the lentiviral pLDPuro-hsnSR100N (35172, Addgene); pCGN-HA-RbFOX1, carrying human full-length nuclear isoform of RbFOX1 cDNA cloned into pCGN vector (53395, Addgene) from pENTR-A2BP1 (16176, Addgene); pEGFP-rbFOX2, with human full-length nuclear isoform of RbFOX2, was a gift from Nicolas Charlet-Berguerand (Addgene plasmid #63086; http://n2t.net/addgene:63086: RRID:Addgene_63086). SH-SY5Y cells were transfected with LSD1 expression vector (pCGN-HA-LSD1). N2a cells were transfected with RbFOX1 expression vector (pCGN-HA-RbFOX1). In order to generate inducible stable SH-SY5Y cell line that expresses RbFOX1 only in presence of doxycycline (DOX, TetON RbFOX1), we performed a double stable transfection with pTet-On (K1621-A, Clontech) and pTRE2hyg-HA-RbFOX1 plasmids, the latter produced by cloning HA-RbFOX1 sequence, obtained through high-fidelity PCR from pCGN-HA-RbFOX1, into pTRE2hyg vector (6255-1, Clontech).

Minigene reporter assay. Minigene reporter assay was performed as described previously (Baralle and Baralle, 2005; Rusconi et al., 2015). The minigenes (hMG2700 WT, archaic MUT hMG2700, lemur MG2700, and MUT lemur MG2700) were transfected alone or together with nSR100 and/or RbFOX1 or RbFOX2 expression plasmids. At 48 h after transfection, RNA was extracted and rqfRT-PCR was conducted using primers that anneal on minigene exons.

Total RNA extraction, RT-PCR, qRT-PCR, rqfRT-PCR. Total RNA extraction from cells and tissue samples was performed using TRIzol reagent (15596026; Invitrogen) according to the manufacturer's protocol. RNA was reverse-transcribed using Maxima H Minus cDNA Synthesis Master Mix with dsDNase kit (M1682; Thermo Fisher Scientific). RT-PCR was conducted with GoTaq G2 Flexi DNA Polymerase (M7805, Promega) following standard PCR protocol. PCR products were separated on 2% agarose gels. Since endogenous E8b-including LSD1 mRNA is present in a very low amount, we exploited touchdown PCR strategy to increase amplification specificity and sensitivity, and we ran 50 cycles of amplification to detect it. E8b expression was quantified using UVITEC Gel Documentation System Essential V6 (Cambridge) and normalized over RPSA.

qRT-PCR analysis was performed on QuantStudio 5 Real-Time PCR System (A28575, Thermo Fisher Scientific) using Power SYBR Green PCR Master Mix (A25742, Applied Biosystem) as described (Spreafico et al., 2018). Gene expression levels were normalized over a proper housekeeping gene (human RPSA, mouse GJA1, and mouse RPSA) and calculated based on the fold change method (2-ΔΔCt). Relative quantity fluorescent PCR (rqfRT-PCR) was conducted using forward primer conjugated with 6-carboxyfluorescein (6-FAM) and a reverse unmodified one, as described (Zibetti et al., 2010). PCR products were mixed together with GeneScan 500 ROX dye Size Standard (4310361, Applied Biosystems) and separated by capillary electrophoresis under denaturing conditions using 3130xl Genetic Analyzer (Applied Biosystems). The amount of each amplified product was quantified using GeneMapper software (RRID:SCR_014290).

An application-specific primer list is provided in Extended Data Table 1-1.

Protein extraction and Western blotting. Total protein extracts were obtained lysing the cells directly with Laemmli's sample buffer 1× supplemented with 2% 2-mercaptoethanol (M6250, Sigma Aldrich) immediately before use (Rusconi et al., 2010). Immunoreactive bands were detected and quantified with UVITEC Alliance Mini HD9 (Cambridge). GAPDH was used as control protein for normalization. Primary and secondary antibodies used are as follows: HA-probe (F-7) mouse mAb (Santa Cruz Biotechnology, RRID:AB_627809); LSD1 (C69G12) rabbit mAb (Cell Signaling Technology, RRID:AB_2070132); GAPDH (D16H11) rabbit mAb (Cell Signaling Technology, RRID:AB_10622025); anti-mouse IgGκ BP-HRP (Santa Cruz Biotechnology, RRID:AB_2687626); and anti-rabbit IgG, HRP-linked whole Ab (GE Healthcare, RRID:AB_772206).

Sanger sequencing of PCR-derived DNA samples. PCR fragment, purified from agarose gel, were sequenced using BigDye Terminator version 3.1 Cycle Sequencing Kit (4337455, Applied Biosystems) and run on 3130xl Genetic Analyzer (Applied Biosystems). Electropherograms were visualized and analyzed with SeqMan Pro package of DNASTAR Lasergene (DNASTAR, RRID:SCR_000283).

Acute social defeat stress (ASDS) and experimental animals. We performed ASDS as described by Italia et al. (2020). During ASDS, 3-month-old male CD1 (RRID:IMSR_CRL:022) aggressor mice were used to defeat 2-month-old male C57BL/6N (RRID:IMSR_CRL:027) WT mice in a two-phase psychosocial stress paradigm. First, the experimental C57BL/6N mouse is forced in a direct interaction with an aggressor CD1 mouse for 5 min (physical stress phase). During the second phase, mice are divided through a perforated Plexiglas barrier and kept in visual and olfactory interaction for 2/7 h (psychological stress phase). Control mice were manipulated, housed in opposite sides of the Plexiglas divider, and roomed in a different place to avoid conditioning. At the end of the psychosocial stress or after 24 h resting phase, control and experimental mice were killed and tissues were collected for molecular analyses. Animals were housed in a SPF animal facility, were kept in an enriched environment, and individually caged only during testing periods. All experimental procedures involving animals followed the Italian Council on Animal Care guidelines (Legislative Decree no. 26, March 2014) and European regulations (2010/63/UE) and were approved by Italian Ministry of Health (no. 322/2018). Every effort was made to accomplish to the "3R" regulations, that is, Reduction of animal number, Refinement of experimental procedures, Replacement with simpler research models.

Human hippocampal samples. Postmortem frozen human tissues were obtained from MRC London Neurodegenerative Diseases Brain Bank and Newcastle Brain Tissue Resource and from routine autopsy at Arcispedale Maria Nuova in Reggio Emilia, Italy (University of Milan Ethic Committee protocol no. 40-18 and Territorial Ethic Committee AUSLRE protocol no. 2019/0004645). Sex, age, cause of death, and postmortem delay were available for each donor, and we scored the agonal state using a 3 point classification based on the cause of death and clinical records (adapted from Monoranu et al., 2009) (Table 1). The quality of RNA extracted from human specimens was assessed using RNA 6000 Nano Chips on Agilent 2100 bioanalyzer measuring RNA integrity number (RIN), which set between 4.6 and 7.5 a range declared previously (Le François et al., 2018) as sufficient for our analyses purpose.

Quantification of LSD1 transcripts expression. We estimated the expression of LSD1 transcripts in HeLa cells using RNA-seq bulk data already available in GEO repository (GSE86148). We considered the following samples: GSM2295861, GSM2295862, and GSM2295876 for scramble; GSM2295864, GSM2295865, and GSM2295866 for UPF1 KD; and GSM2295885, GSM2295886, and GSM2295887 for double KD SMG6-SMG7. We quantified the transcripts using Salmon 1.4.0 (Patro et al., 2017) (in selective alignment mode with default parameters) to increase the accuracy and minimizing the confounding effects of partially overlapping transcriptional isoforms. The salmon index was built using as reference transcriptome GENCODE version 29 considering four isoforms for LSD1 transcripts: ENST00000465864.2, ENST00000685102.1, and the variants of these transcripts with the elongation of the exon E9 (LSD1-E8/E9-long and LSD1-E2a+E8/E9-long; exon coordinate chr1:23068067-23068681). The relative abundances of individual transcript isoforms were calculated to analyze the LSD1 transcriptional dynamics across different conditions (scr, UPF1 KD, and dKD SMG6-SMG7). Briefly, the percentage of the ratio between each LDS1 transcript abundance (TPM) and the total abundance of all LSD1 transcripts was performed.

Experimental design and statistical analyses. For all figures, results are presented with error bars as ± SEM, and the *n* for each condition indicates the number of experimental replicates. For experiments performed in cell cultures, two independent samples from at least three cultures were analyzed. For experiments performed on human postmortem brain specimens, we analyzed 17 hippocampal and 6 cerebellar samples. For ASDS, 4 or 5 C57BL/6N mice were used for each experimental condition. Statistical analyses were performed using GraphPad PRISM 9.0 software (RRID:SCR_002798). For single comparisons, unpaired Student's *t* test was performed when data followed a normal distribution (CHX treatment in SK-N-BE, COV434, and N2a cell lines; DOX treatment in SH-SY5Y TetOn and TetOn RbFOX1 clones and in N2a cells; overall E8a inclusion percentage in hMG2700-derived transcripts in nSR100 and nSR100+RbFOX1 overexpression conditions), while a Mann–Whitney test was performed for those that did not (LSD1 overexpression in SH-SY5Y). Normality was determined using a Shapiro–Wilk normality test. For comparisons between matched data, we performed a paired Student's *t* test (human hippocampal and cerebellar samples analysis). For comparison among >2 conditions (E8b inclusion percentage in hMG2700-derived transcripts on RbFOX1 or RbFOX2 overexpression; CHX treatment in SH-SY5Y cells; ASDS), a one-way ANOVA was performed and results were corrected for multiple comparisons (Tukey's multiple comparisons test). Two-way ANOVA was performed for comparison between MG and MG-E8b after nSR100 or nSR100+RbFOX1 overexpression. Results were corrected for multiple comparisons (Sidak's multiple comparisons test). $p < 0.05$ was considered statistically significant.

Table 1. Postmortem brain samples information

Tissue	ID	Gender	Age (yr)	Origin	Cause of death	Agonal state (1-3)	PMD (h)
Hippocampus	hHIPPO C18	M	21	Dedicated study	Accident	1	75
	hHIPPO C02	M	25	Dedicated study	Intoxication	3	44
	hHIPPO C20	M	35	Dedicated study	Accident	1	50
	hHIPPO C12	M	39	Dedicated study	Hypersensitivity reaction	3	50
	hHIPPO C09	M	44	Dedicated study	Ischemic heart disease	1	30
	hHIPPO C14	M	49	Dedicated study	Ischemic heart disease	1	68
	hHIPPO C17	M	50	Dedicated study	Ischemic heart disease	1	60
	hHIPPO C04	F	53	Dedicated study	Sepsis	3	28
	hHIPPO C11	M	54	Dedicated study	Ischemic heart disease	1	30
	hHIPPO C13	F	56	Dedicated study	Accident	1	27
	hHIPPO C22	F	60	Dedicated study	Ischemic heart disease	1	80
	hHIPPO C07	M	66	Dedicated study	Ischemic heart disease	1	26
	hHIPPO C08	F	71	Dedicated study	Pulmonary embolism	3	70
	hHIPPO C10	M	71	Dedicated study	Ischemic heart disease	1	24
	hHIPPO C25	M	73	MRC Brain Bank	Cancer	3	23
	hHIPPO C01	F	77	Dedicated study	Accident	1	72
	hHIPPO C27	M	78	MRC Brain Bank	Infection	3	24
Cerebellum	hCB 01	M	77	MRC Brain Bank	Cancer	3	1
	hCB 02	M	78	MRC Brain Bank	Infection	3	24
	hCB 03	F	80	MRC Brain Bank	Cancer	3	22
	hCB 04	M	87	NBTR	Renal failure	2	8
	hCB 05	F	92	MRC Brain Bank	Natural death	2	9
	hCB 06	F	94	NBTR	Ischemic heart disease	1	15

PMD, Postmortem delay; Dedicated study, University of Milan Ethic Committee Protocol 40-18 and Territorial Ethic Committee AUSLRE Protocol 2019/0004645; MRC Brain Bank, MRC London Neurodegenerative Diseases Brain Bank; NBTR, Newcastle Brain Tissue Resource.

Results

RbFOX1 promotes the alternative usage of a cryptic 3′ AG splice site in LSD1 gene generating additional splicing isoforms

Considering that RbFOX1 is a brain-enriched RNA-binding protein implicated in homeostatic splicing regulation (Lee et al., 2009; Gehman et al., 2011; Amir-Zilberstein et al., 2012), we hypothesized its possible role in controlling, alongside nSR100 and NOVA1 (Rusconi et al., 2015), alternative splicing of LSD1 exon E8a, and the consequent generation of neuroLSD1. RbFOX1 exerts its function as splicing factor binding the conserved consensus motif (U)GCAUG within introns. In the human *LSD1* INT8a-9 (downstream of exon E8a), we identified two RbFOX1 consensus sequences very close to each other (Fig. 1*A*). To evaluate RbFOX1 contribution to E8a splicing, we exploited a minigene reporter assay (Baralle and Baralle, 2005; Rusconi et al., 2015). We cloned the inherent 2749 nucleotide-long human genomic region (chr1:23065790-23068538) in pBSplicing plasmid, spanning from ~400 bp upstream of exon E8a to the whole downstream INT8a-9 (hMG2700).

We cotransfected the hMG2700 reporter plasmid with or without the E8a master regulator nSR100 (pCDNA3.1 Flag-nSR100) in SH-SY5Y cells and analyzed all minigene-derived transcripts using rqfRT-PCR with vector-specific primers (Baralle et al., 2003; Baralle and Baralle, 2005) (Fig. 1*B*). The minigene-derived transcript is identified by a PCR fragment of 246 bp (MG) (Fig. 1*B*). As previously shown, Flag-nSR100 cotransfection highlights a second peak of 258 bp relative to a second minigene-derived transcript that includes 12-bp-long exon E8a (MG-E8a) (Fig. 1*B*). Unexpectedly, when contransfecting the minigene with HA-RbFOX1 alone, an unknown transcript appeared, including additional 77 bp to the minigene-derived transcript (total of 323 bp corresponding to MG + 77bp). When HA-RbFOX1 is cotransfected with Flag-nSR100, the novel 77 bp additional fragment is included within MG and MG-E8a transcripts. Hence, a total of four peaks are detectable, which include MG (peak 1), MG-E8a (peak 2), MG + 77bp (peak 3), and another transcript MG-E8a + 77bp of 335 bp (peak 4) (Fig. 1*B*). To assess the nature of this 77-bp-long fragment, we sequenced the PCR product relative to the MG + 77bp and the MG-E8a + 77bp amplicons. This analysis unraveled the existence of a novel *LSD1* alternative exon, whose splicing is promoted by RbFOX1 that we named exon E8b (Fig. 1*A*). MG-E8a (peak 2), MG-E8b (peak 3), and MG-E8a+E8b (peak 4) corresponding peaks can be detected also without nSR100 and RbFOX1 cotransfection when a higher amount of amplified DNA is loaded, which however leads to peak 1 and 2 saturation (Fig. 1*B*′). Exon E8b seems to represent a true *cryptic* exon with acceptor (AG) and donor (GU) splice sites that includes an in-frame stop codon potentially leading to the degradation of endogenous LSD1 transcripts via NMD (Fig. 1*A*). Notably, exon E8b has never been reported. This is presumably because of rapid physiological NMD, a cellular process that requires protein synthesis (Chang et al., 2007). We could easily identify minigene-derived transcripts including exon E8b because transcripts generated from this plasmid do not assemble ribosomal subunits, due to the designed absence of the AUG codon in pBSplicing vector (Baralle and Baralle, 2005); hence, they are not subjected to NMD (Rusconi and Battaglioli, 2018).

RbFOX1 is highly enriched in brain and muscles, while in all other tissues an *RbFOX1* paralog, namely, *RbFOX2*, is prevalent (Kuroyanagi, 2009). Indeed, RbFOX1 and RbFOX2 RNA-binding domains share the same target sequence (UGCAUG) (Kuroyanagi, 2009). We therefore tested the ability of RbFOX2 to induce E8b exonization in hMG2700 when overexpressed, showing that also RbFOX2 is able to induce E8b inclusion in minigene transcripts. However, RbFOX2 promotes E8b exonization 4 times less efficiently compared with RbFOX1 (Fig. 1*C*, CTR vs RbFOX1, 0.74 ± 0.22 vs 47.18 ± 1.35, $^{****}p < 0.0001$; CTR vs RbFOX2, 0.74 ± 0.22 vs 11.83 ± 0.58, $^{****}p < 0.0001$;

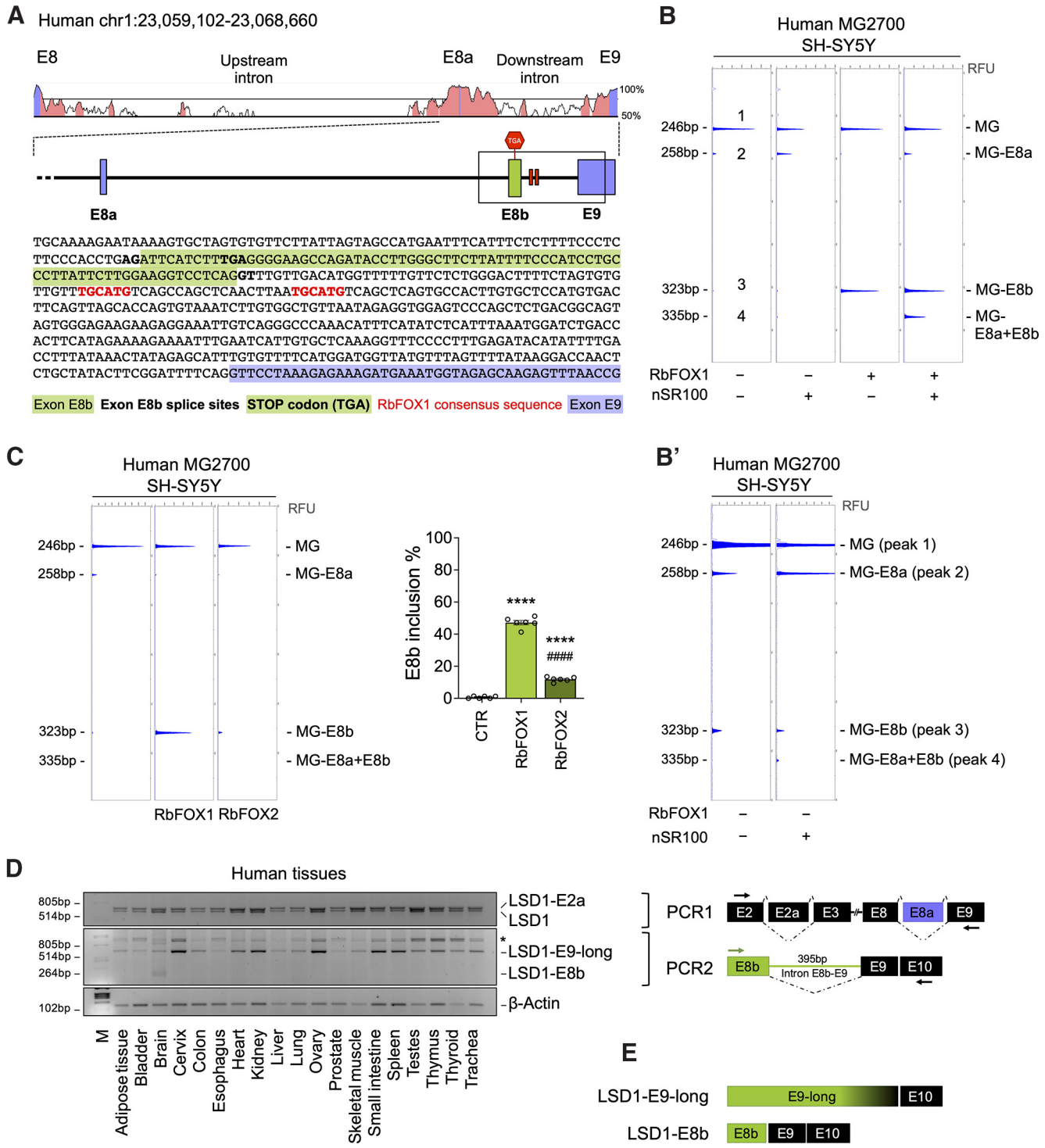

Figure 1. RbFOX1 regulates the inclusion of a novel LSD1 cryptic exon (E8b) in minigene reporter assays. In human tissues, this cryptic exon is present in two versions: brain-specific E8b and ubiquitously expressed E9-long. ***A***, The "peaks and valley" graph, generated with Genome Vista browser, shows a high degree of conservation among mammalian species at specific genomic coordinates (human GRCh38/hg38) of *LSD1* INT8-9. The enlarged schematic representation of exon E8a downstream intron shows the localization of E8a (purple), E8b (green), the two RbFOX1 consensus motifs (red), and E9 (purple). DNA sequence of exon E8b (highlighted in green) and its intronic flanking regions are reported. Embedded premature (TGA) STOP codon is in bold. Bold represents E8b splice sites. Red represents RbFOX1 consensus motifs. Purple represents first 110 nucleotide of exon E9. ***B***, GeneMapper capillary gel electrophoresis analysis of minigene amplicons by rqfRT-PCR performed SH-SY5Y cells transfected with hMG2700 alone, or cotransfected with nSR100 and/or RbFOX1. The transfection of hMG2700 alone generates the minigene minimal transcript (MG, 246 bp, peak 1) and a second transcript including the 12 nt-long E8a (MG-E8a, 246 + 12 = 258 bp, peak 2) whose expression is increased by nSR100 transfection. After RbFOX1 transfection, unexpected splicing event entails exonization of a further 77-bp-long LSD1 intronic region (MG-E8b, 246 + 77 = 323 bp, peak 3), the exon E8b. On nSR100 cotransfection, exon E8b can also be included in E8a-containing minigene transcripts (MG-E8a+E8b, 246 + 12 + 77 = 335 bp, peak 4). ***B'***, By loading a higher amount of minigene PCR products on the capillary electrophoresis, regardless the consequent saturation of the minigene-derived transcript without alternative exons (peak 1), E8a and E8b corresponding peaks (peak 2 and 3) appeared in the electropherogram trace, showing that E8a and E8b, respectively, are included in minigene-derived transcripts also when nSR100 and RbFOX1 are not overexpressed. Left, When nSR100 is overexpressed, E8a+E8b-including isoform appears (peak 4) in addition to MG-E8b (peak 3). ***C***, GeneMapper capillary gel electrophoresis analysis of minigene amplicons by rqfRT-PCR performed in SH-SY5Y cells transfected with hMG2700 alone (CTR), or cotransfected with RbFOX1 or RbFOX2. The transfection of hMG2700 alone generates the minigene minimal transcript

RbFOX1 vs RbFOX2, 47.18 ± 1.35 vs 11.83 ± 0.58, $^{\#\#\#\#}p < 0.0001$), suggesting that RbFOX1 and RbFOX2 are not fully redundant as LSD1 regulators.

In order to verify the existence of LSD1-E8b isoforms *in vivo*, we analyzed a panel of human tissues. LSD1 can be visualized with two RT-PCR bands corresponding to LSD1 with or without alternative exon E2a (E8a cannot be resolved being only 12 nt in length) (Fig. 1*D*, PCR1). PCR1 does not show any further amplicon, except the two above mentioned, including LSD1 and LSD1-E2a related sequences. For this reason, we decided to modify the PCR probes to increase isoform selectivity and detectability. Hypothesizing that transcripts including the further 77 bp could be expressed at very low levels because of a rapid degradation, we designed E8b-specific forward primer and LSD1 E10-annealing reverse primer (PCR2, Fig. 1*D*). With this approach, we successfully detected E8b-including amplicons in the human brain. Interestingly, with PCR2, we also detected in all tissues, a second slower migrating PCR band, which on sequencing resulted to include exon E8b along with its intronic downstream sequences. As such, E9-long novel exon is generated, which comprises E8b sequence together with exonized INT8a-9 and E9 (Fig. 1*D*, right). Thus, the exon E8b identified by minigene experiments (77 bp long) does exist in brain-derived LSD1 transcripts (Fig. 1*D*). However, in all other human tissues analyzed, the E8b GU donor splice site is generally neglected, becoming the dominant donor splice site of exon E9, which makes E9-long prevailingly spliced into LSD1 transcripts. Figure 1*E* shows a schematic representation of the two possible LSD1 alternative exons, respectively, E8b and E9-long highlighted by PCR2.

Taking into consideration that E8b and E9-long have in common the same in-frame stop codon, the two isoforms should be functionally equivalent and both candidates to be subjected to NMD. As both are present in human tissues, although E9-long is more widespread and E8b restricted to the brain, we will refer to E8b/E9-long as the alternative LSD1 exons whose functional significance is studied throughout this work.

Splicing of the cryptic LSD1 exons E8b/E9-long is a higher primates' acquisition

While the genomic region encompassing exons E8a and E8b is not conserved in other vertebrates, in mammals, this intronic sequence is particularly highly conserved (Fig. 1*A*). We proceeded by aligning the identified exon E8b/E9-long sequence among mammals (Fig. 2*A*). Interestingly, our analysis showed that exon E8b/E9-long acceptor splice site (AG dinucleotide) is only present in the genome of higher primates, suggesting that E8b/E9-long splicing is restricted to these species. To confirm this assumption, we performed exon E8b/E9-long specific PCR on cDNA obtained from a representative panel of nonprimates (rodents), lower primates (nonprimate monkeys, prosimians), and higher primates (great apes and humans) tissues (Fig. 2*B*). As E8b/E9-long inclusion in LSD1 transcripts is a ubiquitous process, we used cDNA from the mouse hippocampus, fibroblast cell lines from lemur (*Eulemur fulvus* 1 [EFU1], *Lemur catta* 1 [LCA1]), lymphoblast cell line of MMU, and human hippocampus. Two different RT-PCR strategies were performed: the PCR2, already described above, and a third PCR using a forward primer specifically annealing to LSD1-E7 and the reverse primer on exon E8b (PCR3) (Fig. 2*B*). As expected, from both analyses emerged that only those mammalian species holding the E8b acceptor splice site (i.e., higher primates) show exon E9-long inclusion in LSD1 transcripts (Fig. 2*B*). While in the human hippocampal samples PCR3 generates two amplicons (including E8b with or without E8a), in the MMU lymphoblast samples, only one PCR product was present. This is because the upper band includes neurospecific LSD1 exon E8a sequences that are not expressed in lymphoblast. As positive control, we assayed the presence of LSD1 transcripts with PCR1, as described in Figure 1*D*. These data indicate that the A to G substitution creates in all higher primates a new acceptor splice site for E8b/E9-long inclusion (Fig. 2*A*). To unambiguously demonstrate that such a genome modification is per se necessary to exonize E8b, we mutagenized the acceptor splice site AG in the hMG2700, back into the *archaic* AA to re-create the lower primate layout. Notably, this single mutation impedes E8b exonization (Fig. 2*C*) also when RbFOX1 is overexpressed. In order to investigate whether AG dinucleotide was also sufficient to induce E8b/E9-long splicing, we cloned lemur genomic sequences corresponding to the human MG2700 and mutagenized the 3′ acceptor splice site of E8b/E9-long (the AA dinucleotide) into AG (Fig. 2*D*). Regardless of RbFOX1 overexpression, we did not observe E8b inclusion in the mutagenized lemur minigene. This experiment indicates that AG dinucleotide is necessary but not sufficient to promote E8b/E9-long exonization. Other E8b-flanking genomic sequences among the few which differ between lemur and simiiformes, must be necessary but not sufficient for E8b inclusion.

Exon E8b/E9-long inclusion regulates LSD1 expression via NMD

Near the 5′ end of exon E8b/E9-long, a premature stop codon is present (Fig. 2*A*). Hence, we investigated the ability of its inclusion to mediate LSD1 transcript degradation through NMD. To inhibit NMD, we treated human and rodent cell lines with a compound capable of blocking protein synthesis, such as CHX. We applied CHX for 6 and 8 h, scoring LSD1 transcripts increase by qRT-PCR. Notably, NMD inhibition increased total LSD1 transcripts in the human neuroblastoma cell line SH-SY5Y (Fig. 3*A*, LSD1 CTR vs CHX 6 h, 0.94 ± 0.05 vs 1.46 ± 0.16, $^{**}p = 0.0073$; CTR vs CHX 8 h, 0.94 ± 0.05 vs 1.36 ± 0.14, $^{*}p = 0.0383$). As positive control, we measured in SH-SY5Y a transcript known to undergo NMD, namely, PRKCA (Cardamone et al., 2017) (Fig. 3*A*, PRKCA CTR vs CHX 6 h, 0.85 ± 0.17 vs 2.05 ± 0.20, $^{*}p = 0.0261$; CTR vs CHX 8 h, 0.85 ± 0.17 vs 2.50 ± 0.32, $^{**}p = 0.0061$). We also analyzed the specific modulation of E8b/E9-long-including LSD1 transcripts on CHX treatment and observed more than a fourfold increase of this isoform mRNA when NMD is inhibited (Fig. 3*B*, LSD1-E8b/E9-long CTR vs CHX 6 h, 1.02 ± 0.07 vs 4.53 ± 0.48, $^{***}p = 0.0003$; CTR vs CHX 8 h, 1.02 ± 0.07 vs 4.98 ± 0.61, $^{***}p = 0.0001$). Thus, on NMD inhibition, E8b/E9-long including transcripts appear to increase more than total LSD1 transcripts (compare Fig. 3*B* with Fig. 3*A*), which is consistent with E8b/E9-long splicing responsible for LSD1 transcript degradation. Indeed, among

←

(MG, 246 bp) and a second transcript including the 12-nt-long E8a (MG-E8a, 246 + 12 = 258 bp). Upon transfection, both RbFOX1 and RbFOX2 induce the exonization of E8b (MG-E8b, 246 + 77 = 323 bp). Comparison of E8b inclusion in minigene-derived transcripts on RbFOX1 and RbFOX2 overexpression ($F_{(2,15)} = 780.3$, $p < 0.0001$). Data are mean ± SEM. *Compared with CTR. $^{\#}$Compared with RbFOX1. $^{****}p < 0.0001$, $^{\#\#\#\#}p < 0.0001$, one-way ANOVA, Tukey's *post hoc* test. ***D***, panLSD1-isoforms RT-PCR (top, PCR1) and LSD1-E8b specific RT-PCR (middle, PCR2) performed in human tissues (β-actin is shown). PCR strategies are indicated. *An aspecific band. ***E***, Schematic representation of PCR2 amplicons. In human tissues, the prevailing isoform is LSD1-E9-long; LSD1-E8b is only present in brain tissues.

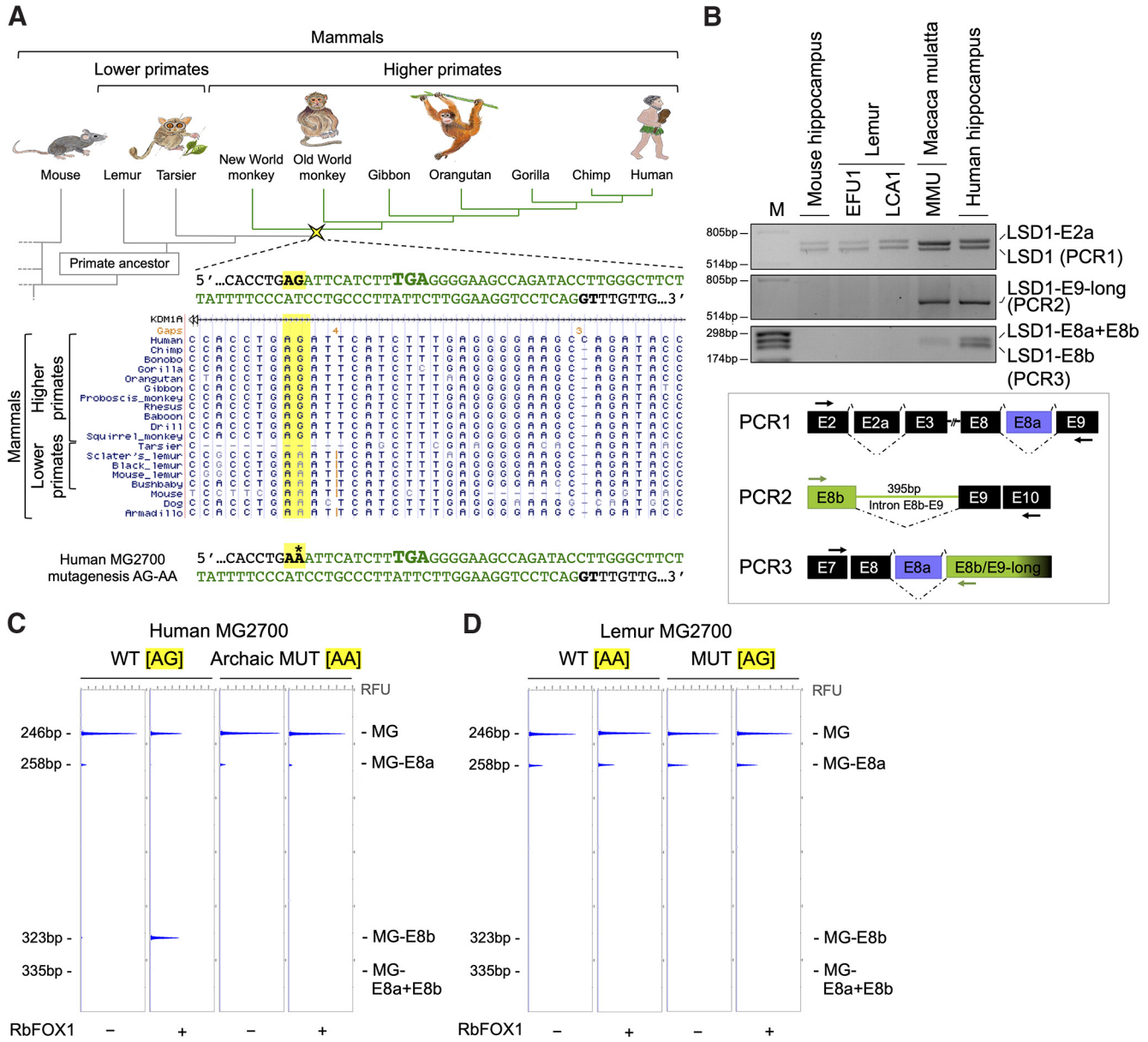

Figure 2. Exon E8b/E9-long inclusion is a higher primate acquisition. ***A***, Multiple alignment of the human *LSD1* exon E8b/E9-long 5′ end in mammals. E8b/E9-long AG splice acceptor site (highlighted in yellow) is only present in higher primates. ***B***, LSD1 isoform detections by RT-PCR (PCR1, PCR2, and PCR3) in mRNA extracted from mouse hippocampus, lemur (EFU1, LCA1) fibroblast cell lines, MMU lymphoblast cell line, and human hippocampus. PCR strategies are indicated. PCR3 reverse primer anneals on E8b, amplifying both E8b- and E9-long-including LSD1 isoforms (a schematic view of all LSD1 splicing isoforms is presented in Fig. 6). ***C***, In the *human* minigene MG-2700, mutation of AG E8b acceptor splice site into the archaic AA dinucleotide prevents RbFOX1-mediated E8b exonization. GeneMapper capillary gel electrophoresis analysis of minigene amplicons by rqfRT-PCR performed in SH-SY5Y cells transfected with WT hMG2700 [AG], or mutant hMG2700 [AA] alone, or cotransfected with RbFOX1. ***D***, GeneMapper capillary gel electrophoresis analysis of minigene amplicons by rqfRT-PCR performed in SH-SY5Y cells transfected with WT lemur MG2700 [AA], or mutant lemur MG2700 [AG] alone or cotransfected with RbFOX1.

all LSD1 transcript isoforms, only the fraction including E8b/E9-long exon is prevented by CHX treatment from NMD-induced degradation, supplying a mechanistic explanation for overall increase of total LSD1 isoforms. We repeated these experiments with two other human cell lines (SK-N-BE and COV434), confirming E8b/E9-long-induced LSD1 degradation (not shown). To strengthen the link between exon E8b/E9-long and NMD-mediated decrease of LSD1, we performed the same CHX experiment in a murine cell line, in which E8b/E9-long splicing inclusion cannot occur because of the absence of 3′ AG acceptor splice site. In the murine neuroblastoma cell line N2a, NMD inhibition did not exert any effect on LSD1 transcripts, whereas it increased the levels of a known positive control, namely, HNRNPL (Fig. 3*C*, LSD1 CTR vs CHX 6 h, 0.69 ± 0.18 vs 0.50 ± 0.04, $p = 0.36$; HNRNPL CTR vs CHX 6 h, 1.36 ± 0.20 vs 28.91 ± 2.01, $^{***}p = 0.0002$).

To provide a further proof that LSD1 levels are regulated by NMD via alternative inclusion of E8b/E9-long, we took advantage of available RNA-seq datasets obtained by specific knockdown of NMD-instrumental factors, such as UPF1 and SMG6-7 in HeLa cells (Colombo et al., 2017). With this approach, we observed a modest increase of E8b/E9-long-including LSD1 transcript isoforms (Fig. 3*D*). However, in this cell line, the overall level of E8b/E9-long-including LSD1 transcript is extremely low (not shown), and we could not detect any appreciable

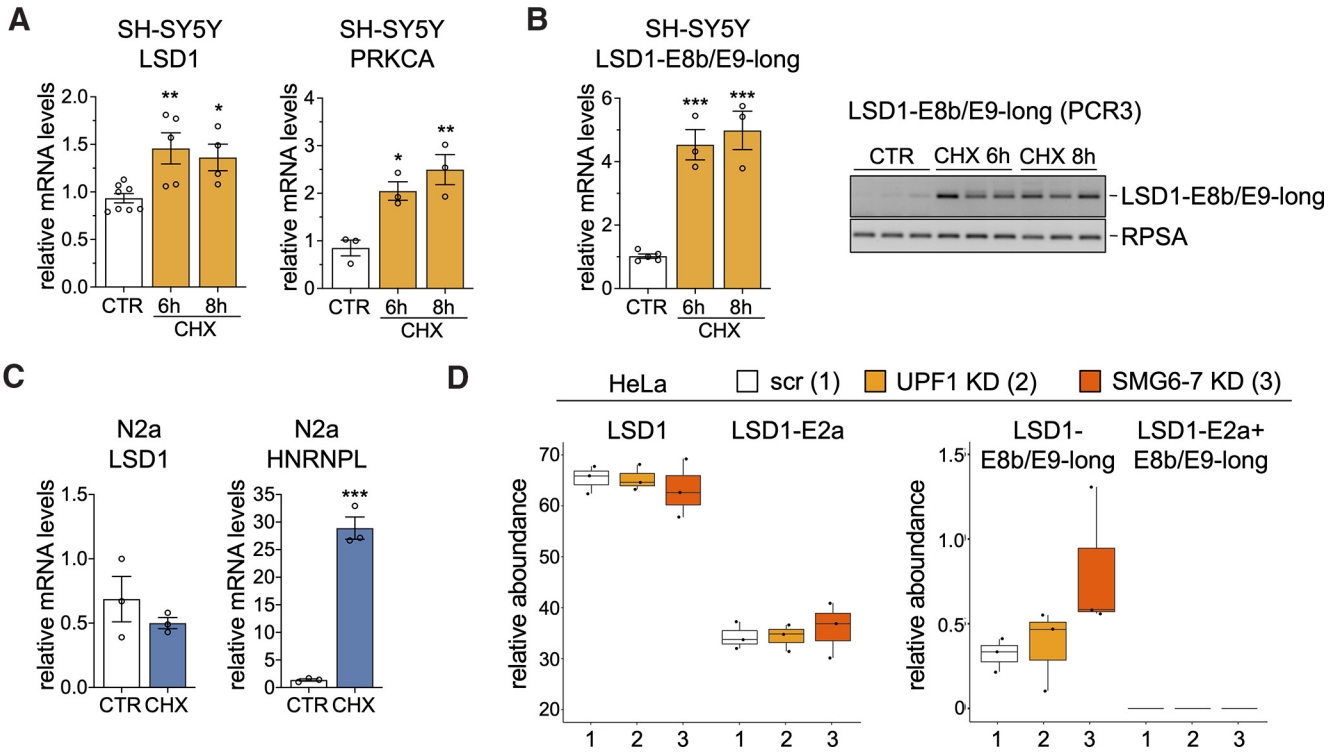

Figure 3. Splicing inclusion of E8b/E9-long in LSD1 mature transcripts causes LSD1 transcript degradation via NMD. ***A***, LSD1 transcript level (normalized over RPSA) on NMD inhibition (CHX, 100 µg/ml for 6/8 h) in human cell line SH-SY5Y assessed by qRT-PCR ($F_{(2,14)} = 7.79$, $p = 0.0053$). PRKCA1 was used as NMD-positive control ($F_{(2,6)} = 13.18$, $p = 0.0064$). ***B***, Representative agarose gel visualization of upstream LSD1-E8b/E9-long specific RT-PCR (PCR3) on SH-SY5Y cell line after CHX treatment and corresponding quantification of LSD1-E8b transcripts, normalized over RPSA ($F_{(2,8)} = 42.02$, $p < 0.0001$). ***C***, LSD1 transcript level (normalized over GJA1) on NMD inhibition in a mouse (N2a) cell line, assessed by qRT-PCR. HNRNPL was used as NMD-positive control. Data are mean ± SEM. Compared with CTR (untreated cells): $*p < 0.05$, $**p < 0.01$, $***p < 0.001$, Student's *t* test for simple comparisons; one-way ANOVA, Tukey's *post hoc* test for multiple comparisons. ***D***, Relative abundance of LSD1 canonical transcripts (LSD1 and LSD1-E2a) and of their variants with E8b/E9-long (LSD1-E8/E9-long and LSD1-E2a+E8/E9-long) in RNA-seq data of UPF1 KD and SMG6-7 kD performed in HeLa cells (Colombo et al., 2017) ($n = 3$ individual for each condition) KD, knock down; scr, scramble. For box-and-whisker plots, the central line, box, and whiskers represent the median, interquartile range from first to third quartiles, and 1.5 × interquartile range, respectively.

modulation of total LSD1 mRNA. This could because of the very low levels of RbFOX1 and RbFOX2 expression in HeLa cells.

Together, these results suggest a novel post-transcriptional mechanism of negative LSD1 regulation, which is restricted to higher primates and humans.

RbFOX1 negatively modulates LSD1 expression via exon E8b/E9-long splicing, ultimately regulating the IEGs

Minigene splicing assays suggested that E8b/E9-long inclusion into mature LSD1 transcripts requires RbFOX1, which seems to be necessary and sufficient to promote LSD1 exon E8b/E9-long alternative splicing in higher primates. To verify whether RbFOX1 regulates LSD1 expression via controlling E8b/E9-long splicing into LSD1 transcripts, we generated a RbFOX1 DOX-inducible cell line. We used SH-SY5Y TetOn cells, stably transfecting pTRE2hyg-HA-RbFOX1 (TetOn RbFOX1). As control, we used SH-SY5Y TetOn parental cell line. At this point, we examined HA-RbFOX1 effects on LSD1 expression at the protein and mRNA levels. Upon DOX treatment, which induces HA-RbFOX1 protein expression, we could observe significant LSD1 protein downregulation compared with its control (Fig. 4*A*, TetOn RbFOX1 CTR vs DOX, 0.93 ± 0.04 vs 0.73 ± 0.04, $*p = 0.0108$). On the contrary, LSD1 protein level did not change in SH-SY5Y TetOn cells with or without DOX (Fig. 4*A*, TetOn CTR vs DOX, 1.12 ± 0.08 vs 1.12 ± 0.08, $p = 0.9989$). Consistently with the proposed NMD-mediated mechanism of LSD1 regulation, also total LSD1 transcript levels, amplified by qRT-PCR using panLSD1 primers, were clearly reduced only in SH-SY5Y TetOn HA-RbFOX1 cells but not in TetOn parental cell line (Fig. 4*B*, TetOn RbFOX1 CTR vs DOX, 1.24 ± 0.15 vs 0.79 ± 0.06, $**p = 0.0055$; TetOn CTR vs DOX, 0.90 ± 0.06 vs 0.93 ± 0.13, $p = 0.7907$). Relevantly, all these results rely on RbFOX1-mediated exonization of LSD1 exon E8b/E9-long, whose inclusion is eventually increased by DOX as evidenced with RT-PCR performed with an exon E8b-specific primer (Fig. 4*C*, TetOn RbFOX1 CTR vs DOX, 0.96 ± 0.15 vs 1.67 ± 0.21, $*p = 0.0165$; TetOn CTR vs DOX, 1.22 ± 0.28 vs 1.07 ± 0.15, $p = 0.6540$). As positive control, DOX-induced RbFOX1 expression modulates alternative splicing of the known RbFOX1 target, NUMA1 (Zhang et al., 2008; Denichenko et al., 2019) (Fig. 4*D*).

LSD1 is a transcriptional regulator of the IEGs (Toffolo et al., 2014; Wang et al., 2015; Rusconi et al., 2016); consistently, its overexpression in SH-SY5Y cell line leads to Egr1 and C-fos downregulation (Fig. 4*E*, VEC vs LSD1 OEX; Egr1, 1.08 ± 0.08 vs 0.77 ± 0.09, $*p = 0.0291$; C-Fos, 1.05 ± 0.08 vs 0.64 ± 0.06, $**p = 0.0012$; Npas4, 1.08 ± 0.12 vs 0.78 ± 0.09, $p = 0.0676$). In order to verify whether RbFOX1-mediated LSD1 downregulation also impacts the expression of LSD1 downstream targets, we measured IEG expression on RbFOX1 induction by DOX treatment. In Figure 4*F*, we show that Egr1, C-Fos, and Npas4 are significantly upregulated on RbFOX1 overexpression. This modulation did not occur in the TetOn parental SH-SY5Y clone (Fig. 4*F*, TetOn RbFOX1, Egr1 CTR vs DOX, 0.92 ± 0.09 vs 1.58 ± 0.15, $**p = 0.0055$; C-Fos CTR vs DOX, 0.75 ± 0.12 vs 1.30 ± 0.10, $**p = 0.0084$; Npas4 CTR vs DOX, 0.95 ± 0.04 vs 1.44 ± 0.21, $*p = 0.0318$; TetOn, Egr1 CTR vs DOX, 0.96 ± 0.09 vs

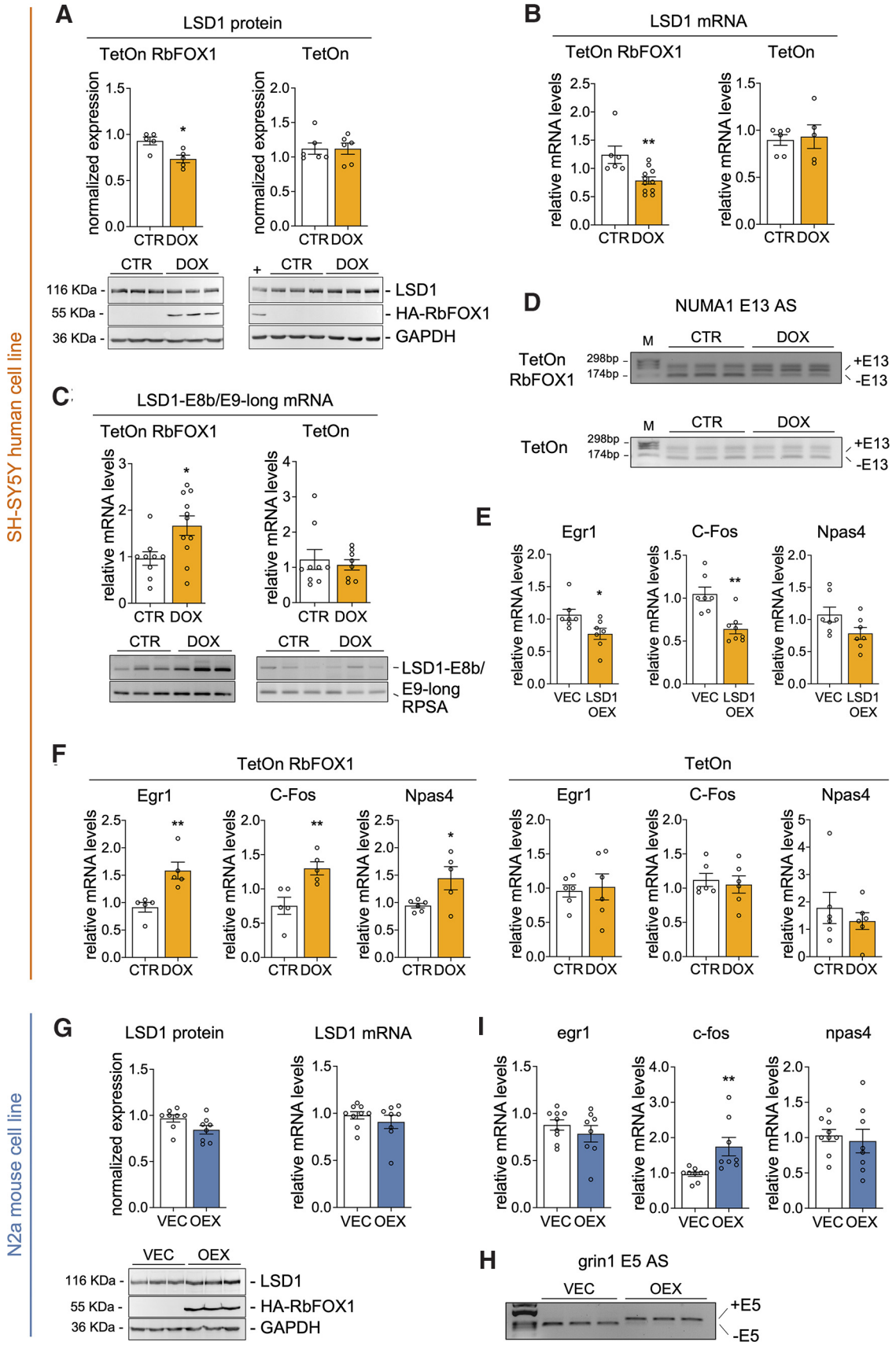

Figure 4. RbFOX1 regulates LSD1 expression through NMD by promoting exon E8b/E9-long inclusion. ***A***, LSD1 protein quantification using anti-LSD1 antibody (normalized over GAPDH) on DOX induction (1 μg/ml for 24 h) of HA-RbFOX1 in SH-SY5Y clonal line (SH-SY5Y TetOn HA-RbFOX1) compared with SH-SY5Y parental line (TetOn). HA antibody was used to visualize RbFOX1 overexpression (+, positive control for HA-RbFOX1 expression). ***B***, LSD1 transcript, assessed by qRT-PCR (normalized over RPSA) in the two SH-SY5Y clones as in ***A***. ***C***, E8b/E9-long-specific RT-PCR quantification over RPSA in the two SH-SY5Y clones as in ***A***. ***D***, RbFOX1 overexpression regulates alternative splicing of NUMA1 exon E13 (known RbFOX1/2 target gene) in SH-SY5Y TetOn

1.02 ± 0.19, $p = 0.7811$; C-Fos CTR vs DOX, 1.12 ± 0.10 vs 1.05 ± 0.13, $p = 0.6822$; Npas4 CTR vs DOX, 1.78 ± 0.57 vs 1.30 ± 0.31, $p = 0.4760$).

Once again, to fortify the link between exon E8b/E9-long and NMD-mediated decrease of LSD1, we overexpressed RbFOX1 in mouse neuroblastoma N2a cell line. This approach did not affect LSD1 level at either the mRNA or the protein level (Fig. 4*G*, LSD1 protein VEC vs RbFOX1 OEX, 0.97 ± 0.04 vs 0.84 ± 0.05, $p = 0.0625$; LSD1 mRNA VEC vs RbFOX1 OEX, 0.98 ± 0.04 vs 0.91 ± 0.07, $p = 0.3862$), although able to modify the splicing of the known RbFOX1 target grin1 (Lee et al., 2009) (Fig. 4*H*). This is again consistent with the absence of a functional E8b/E9-long dinucleotide acceptor splice site in lower mammals (Fig. 2*A*). Remarkably, LSD1 target genes were not modified in mouse N2a cells overexpressing RbFOX1 with the eminent exception of c-fos (Fig. 4*I*, egr1 VEC vs RbFOX1 OEX, 0.88 ± 0.05 vs 0.79 ± 0.09, $p = 0.3722$; c-fos VEC vs RbFOX1 OEX, 0.96 ± 0.06 vs 1.75 ± 0.26, $^{**}p = 0.0074$; npas4 VEC vs RbFOX1 OEX, 1.03 ± 0.08 vs 0.95 ± 0.17, $p = 0.6648$), whose increased level suggests an alternative, LSD1-independent RbFOX1-mediated regulation.

Lsd1 exons E8a and E8b/E9-long are preferentially spliced together impacting LSD1/neuroLSD1 ratio

In mammals *LSD1* intron INT8-9 shows many peculiarities. Indeed, this single intron contains two alternative exons of predicted functional importance, E8a and E8b/E9-long. As discussed until now, inclusion of exon E8b/E9-long can modulate overall LSD1 expression in a neuronal but in principle also in non-neuronal contexts. However, in the brain, exon E8b/E9-long inclusion could have an additional effect that is to fine-tune the LSD1/neuroLSD1 ratio. This could happen if E8b/E9-long were preferentially included in a specific LSD1 isoform (i.e., if E8a and E8b/E9-long were preferentially spliced together).

We quantitatively analyzed minigene splicing experiments performed in SH-SY5Y cells, in which minigene hMG2700 was cotransfected with Flag-nSR100 or with both Flag-nSR100 and HA-RbFOX1 (Fig. 5*A*, left). As previously shown in Figure 1*B*, on Flag-nSR100 overexpression, the MG transcript, including E8a (peak 2) increases and after Flag-nSR100/HA-RbFOX1 cotransfection, the two MG transcripts, including exon E8b alone (peak 3), or together with exon E8a (peak 4) rise. We observed that overall E8a inclusion, calculated as (peak2 + 4)/(peak1 + 2+3 + 4), is only dependent on nSR100 presence, being not modified by RbFOX1 (Fig. 5*A*, middle, nSR100 vs nSR100+RbFOX1, 31.63 ± 1.59 vs 26.85 ± 2.21, $p = 0.0758$). We then examined E8a inclusion frequency in the two different populations of minigene transcripts: those skipping E8b (MG and MG+E8a, peaks 1 and 2) and those including E8b (MG+E8b and MG+E8a/E8b, peaks 3 and 4). E8a frequency within E8b nonincluding and including transcripts was plotted and calculated as peak2/(peak1 + 2) and peak4/(peak3 + 4), respectively (Fig. 5*A*, right, E8a inclusion in nSR100+RbFOX1, MG vs MG-E8b, 16.85 ± 2.41 vs 31.55 ± 1.96, $^{****}p < 0.0001$). From this analysis, we clearly established that E8a is preferentially included together with E8b. Considering that minigene-derived transcripts do not undergo NMD, with this experiment, we foresee that preferential E8a/E8b inclusion should favor NMD-mediated decrease of E8a containing isoforms, namely, neuroLSD1 in the brain.

To further investigate this hypothesis, we studied E8a and E8b/E9-long splicing in human cerebral tissues. We sequenced PCR3 amplicons obtained from human hippocampus to unambiguously confirm the existence of LSD1-E8b/E9-long including or skipping the exon E8a (Fig. 5*B*). Considering that exon E8b/E9-long-including isoforms are present at very low levels *in vivo*, as they are rapidly degraded by NMD, we exploited a strategy based on two specific internally standardized rqfRT-PCR (Zibetti et al., 2010), allowing the former (PCR1), a reliable evaluation of highly expressed LSD1 isoforms and the latter (PCR3) a measure of E8b/E9-long-containing transcripts (Fig. 5*C*). In principle, PCR1 should also amplify E8b/E9-long-containing amplicons, but this is not the case because they fall under the resolution threshold of the PCR. PCR3 (with E7- and E8b/E9-long-annealing forward and reverse primers, respectively) allows the identification of E8a inclusion frequency in E8b/E9-long-containing LSD1 transcripts. We reasoned that, if E8a were included in LSD1 transcripts independently on E8b/E9-long, then E8a inclusion frequency in PCR1 and PCR3 should be identical. Vice versa, if exon E8a is preferentially included together with E8b/E9-long, the E8a percentages should be different in the two PCRs. We conducted PCR1 and PCR3 on RNA extracted from human postmortem hippocampal and cerebellar samples (Table 1), comparing E8a inclusion frequency in total LSD1 transcripts (PCR1) and in E8b/E9-long-containing LSD1 isoforms (PCR3). We observed that neuroLSD1 relative percentage is higher in E8b/E9-long-including *LSD1* transcripts compared with those who do not, both in human hippocampal and cerebellar samples. In the hippocampus, E8a relative percentage in E8b/E9-long-containing LSD1 transcripts is higher compared with E8a inclusion in total LSD1 transcripts (Fig. 5*C*, Total LSD1 vs LSD1-E8b/E9-long, 23.35 ± 1.58 vs 50.71 ± 6.56, $^{**}p = 0.0011$). Similarly, in the cerebellum, relative E8a percentage inclusion in E8b-containing LSD1 transcripts is higher compared with that of total LSD1 transcripts (Fig. 5*C*, Total LSD1 vs LSD1-E8b/E9-long, 58.87 ± 4.21 vs 78.02 ± 4.61, $p = 0.0547$). Individual differences in E8a-E8b/E9-long co-splicing are shown in Figure 5*D*. Thus, also in endogenous human brain-derived transcripts, E8a and E8b/E9-long exons are preferentially spliced together, entailing increased degradation of neuroLSD1 (the *LSD1* isoform including E8a) and affecting LSD1/neuroLSD1 ratio. All this said, we can conclude that, in addition to the above-described RbFOX1-mediated LSD1 general-level modulation, RbFOX1-operated preferential degradation of neuroLSD1 in the human brain represents a further molecular layer of LSD1/neuroLSD1 ratio regulation.

Considering the fundamental role played by LSD1/neuroLSD1 ratio modulation in allowing environmental adaptation to stress and its important readouts on stress-coping and emotional behaviors, these data indicate a new molecular pathway linking RbFOX1 function to stress responses. We here show that the social defeat stress, which significantly elicits LSD1/neuroLSD1 splicing modulation in the

←

RbFOX1 but not in TetOn parental line. ***E***, LSD1 overexpression in SH-SY5Y cells elicits IEG downregulation: qRT-PCR analysis of the IEGs Egr1, C-Fos, and Npas4 (normalized over RPSA) on LSD1 overexpression (LSD1 OEX) in SH-SY5Y cells. ***F***, qRT-PCR analysis shows that RbFOX1 overexpression regulates LSD1 downstream IEGs targets Egr1, c-Fos, and Npas4 (normalized over RPSA) in TetOn HA-RbFOX1 but not in TetOn parental line. ***G***, RbFOX1 does not regulate LSD1 in lower primates. Overexpression of RbFOX1 (OEX) in mouse-derived N2a cell line (24 h) does not affect LSD1 protein level and mRNA expression (VEC, vector). ***H***, RT-PCR analysis of grin1 E5 alternative splicing (AS) on RbFOX1 overexpression (OEX). ***I***, qRT-PCR analysis of the IEGs egr1, c-fos, and npas4 (normalized over RPSA) on RbFOX1 overexpression (OEX) in N2a. In RbFOX1 overexpression experiments, data are mean ± SEM. *Compared with CTR or VEC in SH-SH5Y or N2a cells, respectively. $^{*}p < 0.05$, $^{**}p < 0.01$, Student's *t* test. In LSD1 overexpression experiment, data are mean ± SEM. *Compared with VEC. $^{*}p < 0.05$, $^{**}p < 0.01$, Mann–Whitney test.

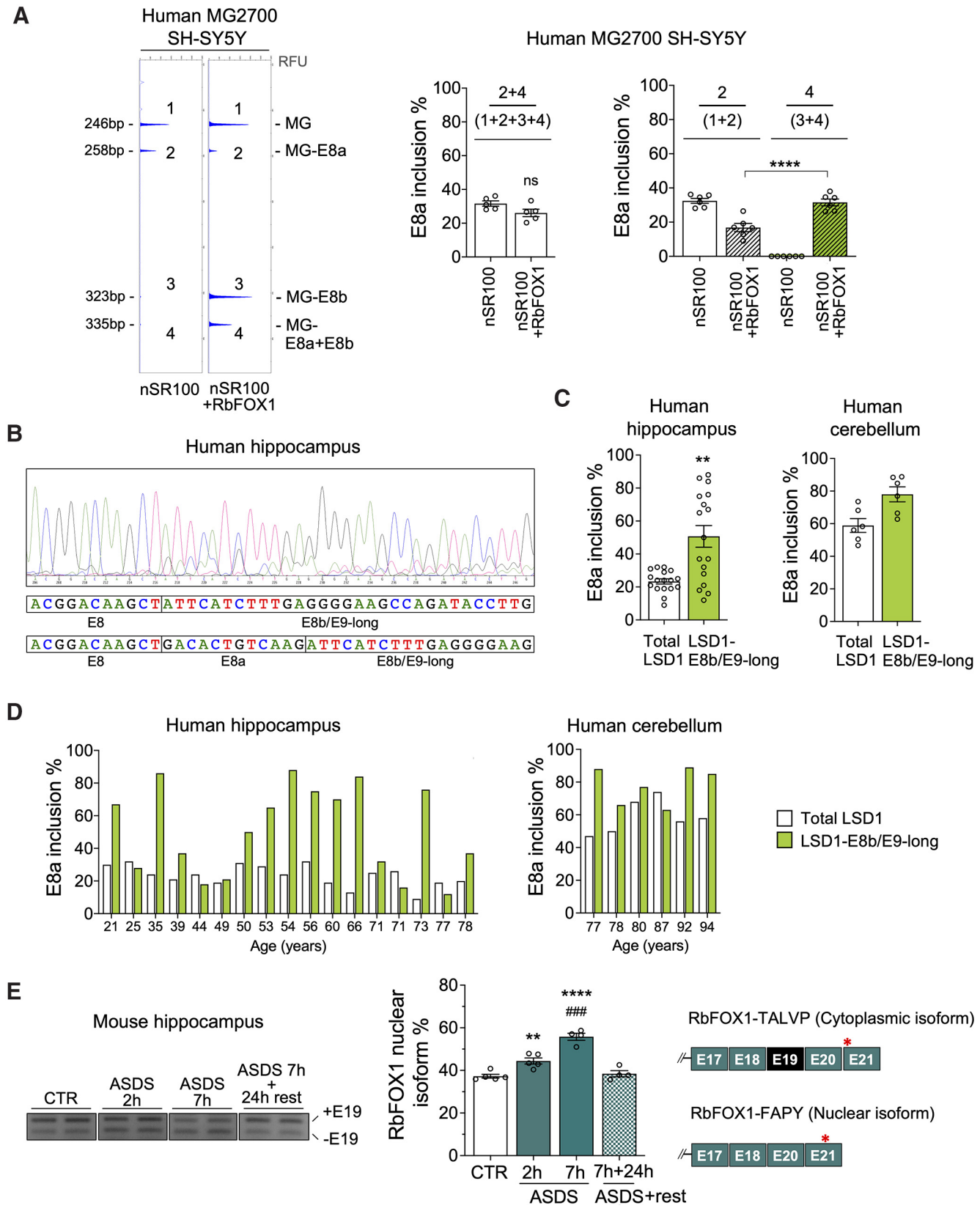

Figure 5. *LSD1* exons E8a and E8b/E9-long are preferentially spliced together impacting LSD1/neuroLSD1 relative ratio. ***A***, Quantification of GeneMapper capillary gel electrophoresis of minigene products amplified by rqfRT-PCR performed SH-SY5Y cells transfected with hMG2700, together with nSR100 alone or with RbFOX1. Overall E8a splicing (left histogram) depends on nSR100 presence and is calculated as follows: (peak2 + 4)/(peak1 + 2+3 + 4). E8a inclusion percentage (right histogram) in E8b nonincluding peak2/(peak1 + 2) and including peak4/(peak3 + 4) transcripts (MG vs MG-E8b: $F_{(1,20)} = 26.65$, $p < 0.0001$; nSR100 vs nSR100+RbFOX1: $F_{(1,20)} = 21.51$, $p = 0.0002$). Data are mean ± SEM. Not significant, $p > 0.05$ (Student's *t* test). ****$p < 0.0001$ (two-way ANOVA Sidak's *post hoc* test). ***B***, Sequence analysis of purified LSD1-related PCR band (PCR3) from human hippocampus shows LSD1 E8-E8b/E9long and E8a-E8b/E9-long splice junctions. ***C***, Quantification of exon E8a (neuroLSD1) inclusion frequency by rqfRT-PCR in total LSD1 transcripts (PCR1, see Fig. 2*B*) and E8b/E9-long-containing LSD1

mouse hippocampus, also shifts the ratio between the nuclear and the cytosolic RbFOX1 isoforms in favor of the nuclear one, namely, RbFOX1-FAPY, involved in splicing regulation (Fig. 5*E*, RbFOX1 nuclear isoform percentage, CTR vs ASDS 2 h, 37.27 ± 0.91 vs 44.42 ± 1.44, $^{**}p = 0.0076$; CTR vs ASDS 7 h, 37.27 ± 0.91 vs 55.79 ± 1.67, $^{****}p < 0.0001$; CTR vs ASDS 7 h + 24 h resting, 37.27 ± 0.91 vs 38.42 ± 1.47, $p = 0.9323$; ASDS 2 h vs ASDS 7 h, 44.42 ± 1.44 vs 55.79 ± 1.67, $^{\#\#\#}p = 0.0002$). Notably, in the mouse brain, the LSD1/neuroLSD1 ratio modulation cannot be contributed by increased nuclear RbFOX1 splicing isoform, indeed, as explained above, RbFOX1-LSD1 functional interaction is a higher primates' acquisition. Nonetheless, the evolutionary conserved (functionally independent) molecular stress-homeostatic pathways of RbFOX1 and LSD1 are functionally linked in higher primates thanks to LSD1 E8b/E9-long exons.

Discussion

In this work, we present the first example of a higher primate-specific target of homeostatic splicing, namely, LSD1, whose alternative isoforms, only in simiiformes, are regulated by RbFOX1. RbFOX1 is the best described homeostatic splicing regulator acting in the mammalian brain as a guardian of neuronal integrity in the face of excessive neuronal activation (Lee et al., 2009; Thalhammer et al., 2020). RbFOX1 plays a major role in neurologic and psychiatric disorders, as described by several genetic studies (Xu et al., 2008; Elia et al., 2010; Lal et al., 2015; Sullivan, 2015; Lee et al., 2016; Fernàndez-Castillo et al., 2020). In the light of LSD1 implications in stress response and emotional behavior (Rusconi et al., 2015, 2016, 2017; Rusconi and Battaglioli, 2018; Longaretti et al., 2020b), our finding of a RbFOX1-LSD1 functional interaction opens a new perspective to further understand pathogenic mechanisms controlled by RbFOX1. *LSD1* gene splicing complexity increases in mammals and higher primates (for details, see Fig. 6). Within this work, we discovered that RbFOX1 positively regulates the choice of an alternative cryptic AG 3′ splice site of LSD1 exon 9, which elongates including the last part of the upstream intron (INT8a-9). We refer to this novel exon as E9-long. In the brain, RbFOX1 also causes the additional appearance of the alternative exon E8b (77 bp long), which shares the same 3′ splice site used by exon E9-long. Thus, E9-long, sharing the first 77 nucleotides with E8b in which a stop codon is present, induces, likewise E8b, LSD1 transcript degradation via NMD. In the human brain, where alternative exon E8a inclusion generates neuroLSD1, a dominant negative isoform unable to repress transcription (Zibetti et al., 2010), we observed a preferential inclusion of E8b/E9-long within neuroLSD1 transcripts. As a result, RbFOX1 concurs, together with NOVA1 and nSR100, to the fine regulation of LSD1/neuroLSD1 relative ratio. While NOVA1 and nSR100 are positive neuroLSD1 regulators, promoting exon E8a inclusion, RbFOX1 induces a preferential neuroLSD1 transcript degradation. A relevant aspect of exon E8b/E9-long is its higher primate-restricted splicing. Indeed, reintroducing the *archaic LSD1* variant by mutating a single nucleotide in the cryptic AG 3′ splice site and converting it to AA, causes loss of E8b/E9-long.

Pathologic domains of altered neuronal excitability and stress susceptibility associate with all those human neurologic and psychiatric disorders featuring a role for RbFOX1, from epilepsy to autism and depression (Lal et al., 2015; Sullivan, 2015; Lee et al., 2016). Consistently, in animal models of stress response, RbFOX1 regulates the hypothalamo-pituitary-adrenal axis (Amir-Zilberstein et al., 2012), whose hyperactivation represents a prominent common biomarker of emotional dysfunction (McEwen and Akil, 2020). It was shown that, on a foot-shock stressful challenge, an increased RbFOX1 transcription reduces corticotropin-releasing hormone levels to terminate hypothalamo-pituitary-adrenal axis activation in the mouse hypothalamus. This work integrated the well-described synaptic homeostatic function of RbFOX1 (Lee et al., 2009) with a behavioral readout in terms of proper regulation of stress response (Amir-Zilberstein et al., 2012). In our work, we widen RbFOX1 implications in stress response, showing that also social defeat stress paradigm increases RbFOX1 nuclear splicing isoform, instrumentally to transient downstream splicing regulation. Thus, in mammals, different types of environmental stress elicit the transient generation of an active nuclear RbFOX1 splicing isoform with homeostatic means. Moreover, these stressful paradigms also entail a transient decrease of the neurospecific LSD1 dominant-negative isoform neuroLSD1, through temporarily decreased inclusion of exon E8a in LSD1 transcripts (Rusconi et al., 2015, 2016; Gerosa et al., 2020; Longaretti et al., 2020a, 2020b), a process that is not controlled by RbFOX1. If we integrate this evidence with the novel finding that restricted to simiiformes, another RbFOX1-related mechanism can specifically decrease neuroLSD1 levels via preferential inclusion of E8b/E9-long within neuroLSD1 isoforms, and consequent selective NMD of neuroLSD1 encoding transcripts, a picture emerges suggesting that this higher primates-specific supplemental mechanism is aimed at an ultimate fine-tuning of LSD1/neuroLSD1 ratio.

Concerning the functional role of RbFOX1-LSD1 interaction, we should keep into consideration an important aspect shared by psychiatric disorders, namely, neuroplasticity issues (Gallo et al., 2018). As modulators of the IEG transcription, LSD1 and neuroLSD1 regulate neuronal plasticity (Wang et al., 2015; Rusconi et al., 2016). In this work, we functionally link RbFOX1 to IEG regulation through LSD1, showing for the first time that RbFOX1, via modulating LSD1 isoforms levels but only in human cells, impacts IEG transcription. Thus, our data indicate that in, higher primates and humans, IEG modulation is endowed with a further regulatory layer, suggesting acquired complexity of cognition and memory-instrumental pathways. IEG regulation must be optimal as their even minimal improper tuning could lead to neurologic and psychiatric issues (Gallo et al., 2018). In humans, the evolutionarily conserved AA to AG INT8a-9 mutation seems therefore to be

←

transcripts (PCR3, see Fig. 2*B*) in human hippocampus ($n = 17$) and in human cerebellum ($n = 6$); average E8a inclusion values are mechanistically evaluated with different quantitative PCRs that are anyway internally standardized (Zibetti et al., 2010). Human postmortem brain specimen description is reported in Table 1. ***D***, Quantification of exon E8a (neuroLSD1) inclusion frequency by rqfRT-PCR in total LSD1 transcripts, in white (PCR1, see Fig. 2*B*), and E8b/E9-long-containing LSD1 transcripts, in green (PCR3, see Fig. 2*B*) in human hippocampus ($n = 17$) and in human cerebellum ($n = 6$) for each individual brain sample. Age (years) for each donor is reported. Data are mean ± SEM. $^{**}p < 0.01$ (paired Student's *t* test). ***E***, Nuclear (RbFOX1-FAPY) and cytoplasmic (RbFOX1-TALVP) RbFOX1 splicing isoforms (Lee et al., 2009; Gehman et al., 2011) are modulated during ASDS in the mouse hippocampus. Quantification of the relative percentage of RbFOX1 nuclear isoform in the mouse hippocampus comparing defeated mice (ASDS) to control ones (CTR) ($n = 4$ or 5 mice per condition) ($F_{(3,14)} = 36.03$, $p < 0.0001$). Agarose gel images are reported: nuclear and cytoplasmic RbFOX1 isoforms are indicated. Data are mean ± SEM. *Compared with CTR. $^{\#}$Compared with ASDS 2 h. $^{**}p < 0.01$, $^{****}p < 0.0001$, $^{\#\#\#}p < 0.001$, one-way ANOVA Tukey's *post hoc* test.

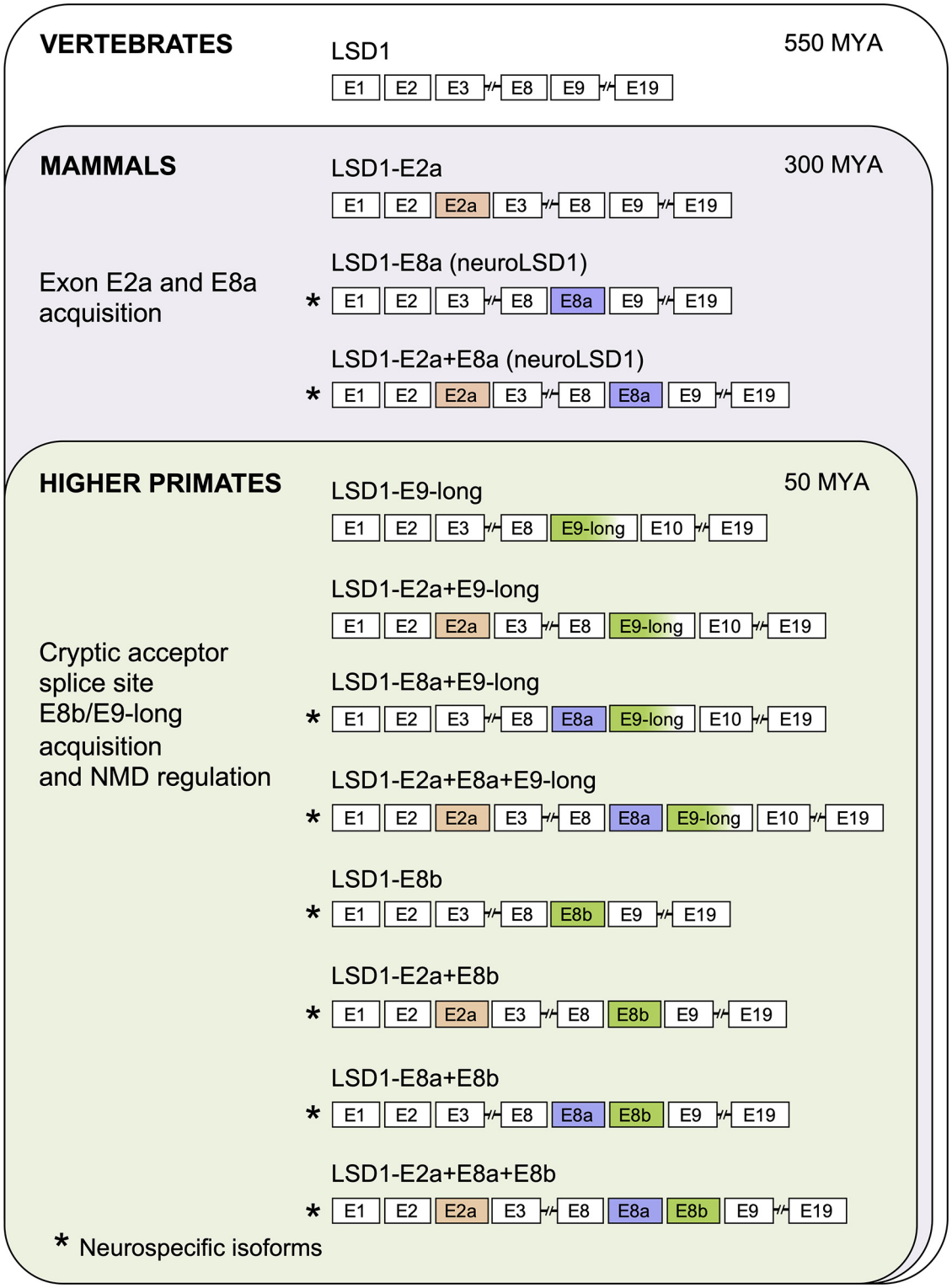

Figure 6. Schematic representation of the human *LSD1* gene splicing complexity at different branches of the evolutionary tree. In nonmammalian vertebrates (in the white subset), a single LSD1 isoform is present. Only in mammals (in the light violet subset), two additional exons (E2a and E8a) appeared whose combinatorial inclusion in mature LSD1 transcripts generate four alternative isoforms (exon E2a is also present in some reptiles and birds). Restricted to higher primates (in the light green subset), another two exons (E8b and E9-long) can be included in mature LSD1 transcripts accounting for the generation of eight additional splicing isoforms. All LSD1 splicing isoforms deriving from the inclusion of alternatively spliced exons E2a (in orange), E8a (in violet) (neuroLSD1), E8b (in green), and E9-long (in green fading to white, E8b+INTE8b-E9+E9) expressed in non-neuronal and neuronal cells are shown. Constitutive exons are shown in white.

necessary for a species-specific IEG expression. Within this context, we believe that fine RbFOX1-mediated LSD1 modulation, playing a relevant role in synapse homeostasis also via the control of the IEGs (Gerosa et al., 2020; Longaretti et al., 2020a,b), could contribute to bridging the gap between RbFOX1 malfunction and psychiatric disorders.

Interestingly, another evolutionary conserved point mutation at the level of an important homeostatic splicing regulator,

NOVA1(Eom et al., 2013), which also participates to the modulation of LSD1 activity (Rusconi et al., 2015), has been recently reported to contribute to Homo sapiens-specific neurodevelopmental processes (Rusconi et al., 2015; Trujillo et al., 2021).

Within this work, we showed that also RbFOX2, a ubiquitously expressed RbFOX1 paralog without an established relationship with psychiatric disorders, can exert a positive regulation of exon E8b inclusion in mature LSD1 transcripts. However, RbFOX2 is capable of a significantly weaker regulation of E8b splicing compared with RbFOX1, which in the brain can be therefore considered among the two, the main LSD1 level modulator, supporting the potential neurologic and neuropsychiatric disease relevance of RbFOX1-LSD1 molecular partnership. Since E9-long is ubiquitously detectable in all analyzed human tissues, including those that do not express RbFOX1, a putative relevance of RbFOX2-LSD1 interaction could be further investigated outside the nervous system. For instance, both LSD1 and RbFOX2 have been reportedly implicated in several human cancers (Braeutigam et al., 2014; Hosseini and Minucci, 2017; Karakaidos et al., 2019). LSD1 overexpression is often associated with negative prognostic parameters; and accordingly, LSD1 represents a promising pharmacological target to restrain tumor de-differentiation ability (Hosseini and Minucci, 2017; Karakaidos et al., 2019). On the other hand, RbFOX2 seems to represent an essential regulator of epithelial-mesenchymal transition (Braeutigam et al., 2014). All this considered, we anticipate RbFOX2 importance in LSD1-regulated cancer progression in metastasis (Karakaidos et al., 2019).

References

Amir-Zilberstein L, Blechman J, Sztainberg Y, Norton WH, Reuveny A, Borodovsky N, Tahor M, Bonkowsky JL, Bally-Cuif L, Chen A, Levkowitz G (2012) Homeodomain protein otp and activity-dependent splicing modulate neuronal adaptation to stress. Neuron 73:279–291.

Baralle D, Baralle M (2005) Splicing in action: assessing disease causing sequence changes. J Med Genet 42:737–748.

Baralle M, Baralle D, De Conti L, Mattocks C, Whittaker J, Knezevich A, Ffrench-Constant C, Baralle FE (2003) Identification of a mutation that perturbs NF1 agene splicing using genomic DNA samples and a minigene assay. J Med Genet 40:220–222.

Braeutigam C, Rago L, Rolke A, Waldmeier L, Christofori G, Winter J (2014) The RNA-binding protein Rbfox2: an essential regulator of EMT-driven alternative splicing and a mediator of cellular invasion. Oncogene 33:1082–1092.

Cardamone G, Paraboschi EM, Rimoldi V, Duga S, Soldà G, Asselta R (2017) The characterization of GSDMB splicing and backsplicing profiles identifies novel isoforms and a circular RNA that are dysregulated in multiple sclerosis. Int J Mol Sci 18:576.

Chang YF, Imam JS, Wilkinson MF (2007) The nonsense-mediated decay RNA surveillance pathway. Annu Rev Biochem 76:51–74.

Colombo M, Karousis ED, Bourquin J, Bruggmann R, Mühlemann O (2017) Transcriptome-wide identification of NMD-targeted human mRNAs reveals extensive redundancy between SMG6- and SMG7-mediated degradation pathways. RNA 23:189–201.

Denichenko P, Mogilevsky M, Cléry A, Welte T, Biran J, Shimshon O, Barnabas GD, Danan-Gotthold M, Kumar S, Yavin E, Levanon EY, Allain FH, Geiger T, Levkowitz G, Karni R (2019) Specific inhibition of splicing factor activity by decoy RNA oligonucleotides. Nat Commun 10:1590.

Elia J, et al. (2010) Rare structural variants found in attention-deficit hyperactivity disorder are preferentially associated with neurodevelopmental genes. Mol Psychiatry 15:637–646.

Eom T, Zhang C, Wang H, Lay K, Fak J, Noebels JL, Darnell RB (2013) NOVA-dependent regulation of cryptic NMD exons controls synaptic protein levels after seizure. Elife 2:e00178.

Fernàndez-Castillo N, Gan G, van Donkelaar MM, Vaht M, Weber H, Retz W, Meyer-Lindenberg A, Franke B, Harro J, Reif A, Faraone SV, Cormand B (2020) RBFOX1, encoding a splicing regulator, is a candidate gene for aggressive behavior. Eur Neuropsychopharmacol 30:44–55.

Gallo FT, Katche C, Morici JF, Medina JH, Weisstaub NV (2018) Immediate early genes, memory and psychiatric disorders: focus on c-Fos, Egr1 and Arc. Front Behav Neurosci 12:79.

Gehman LT, Stoilov P, Maguire J, Damianov A, Lin CH, Shiue L, Ares M, Mody I, Black DL (2011) The splicing regulator Rbfox1 (A2BP1) controls neuronal excitation in the mammalian brain. Nat Genet 43:706–711.

Gerosa L, Grillo B, Forastieri C, Longaretti A, Toffolo E, Mallei A, Bassani S, Popoli M, Battaglioli E, Rusconi F (2020) SRF and SRFΔ5 splicing isoform recruit corepressor LSD1/KDM1A modifying structural neuroplasticity and environmental stress response. Mol Neurobiol 57:393–407.

Guan JS, Haggarty SJ, Giacometti E, Dannenberg JH, Joseph N, Gao J, Nieland TJ, Zhou Y, Wang X, Mazitschek R, Bradner JE, DePinho RA, Jaenisch R, Tsai LH (2009) HDAC2 negatively regulates memory formation and synaptic plasticity. Nature 459:55–60.

Hosseini A, Minucci S (2017) A comprehensive review of lysine-specific demethylase 1 and its roles in cancer. Epigenomics 9:1123–1142.

Iijima T, Wu K, Witte H, Hanno-Iijima Y, Glatter T, Richard S, Scheiffele P (2011) SAM68 regulates neuronal activity-dependent alternative splicing of neurexin-1. Cell 147:1601–1614.

Irimia M, Weatheritt RJ, Ellis JD, Parikshak NN, Gonatopoulos-Pournatzis T, Babor M, Quesnel-Vallières M, Tapial J, Raj B, O'Hanlon D, Barrios-Rodiles M, Sternberg MJ, Cordes SP, Roth FP, Wrana JL, Geschwind DH, Blencowe BJ (2014) A highly conserved program of neuronal microexons is misregulated in autistic brains. Cell 159:1511–1523.

Italia M, Forastieri C, Longaretti A, Battaglioli E, Rusconi F (2020) Rationale, relevance, and limits of stress-induced psychopathology in rodents as models for psychiatry research: an introductory overview. Int J Mol Sci 21:7455.

Karakaidos P, Verigos J, Magklara A (2019) LSD1/KDM1A, a gate-keeper of cancer stemness and a promising therapeutic target. Cancers (Basel) 11:1821.

Kuroyanagi H (2009) Fox-1 family of RNA-binding proteins. Cell Mol Life Sci 66:3895–3907.

Lal D, Pernhorst K, Klein KM, Reif P, Tozzi R, Toliat MR, Winterer G, Neubauer B, Nürnberg P, Rosenow F, Becker F, Lerche H, Kunz WS, Kurki MI, Hoffmann P, Becker AJ, Perucca E, Zara F, Sander T, Weber YG (2015) Extending the phenotypic spectrum of RBFOX1 deletions: sporadic focal epilepsy. Epilepsia 56:e129–e133.

Le François B, Zhang L, Mahajan GJ, Stockmeier CA, Friedman E, Albert PR (2018) A novel alternative splicing mechanism that enhances human 5-HT1A receptor RNA stability is altered in major depression. J Neurosci 38:8200–8210.

Lee JA, Tang ZZ, Black DL (2009) An inducible change in Fox-1/A2BP1 splicing modulates the alternative splicing of downstream neuronal target exons. Genes Dev 23:2284–2293.

Lee JA, Damianov A, Lin CH, Fontes M, Parikshak NN, Anderson ES, Geschwind DH, Black DL, Martin KC (2016) Cytoplasmic Rbfox1 regulates the expression of synaptic and autism-related genes. Neuron 89:113–128.

Longaretti A, Forastieri C, Gabaglio M, Rubino T, Battaglioli E, Rusconi F (2020a) Termination of acute stress response by the endocannabinoid system is regulated through LSD1-mediated transcriptional repression of 2-AG hydrolases ABHD6 and MAGL. J Neurochem 155:98–110.

Longaretti A, et al. (2020b) LSD1 is an environmental stress-sensitive negative modulator of the glutamatergic synapse. Neurobiol Stress 13:100280.

McEwen BS, Akil H (2020) Revisiting the stress concept: implications for affective disorders. J Neurosci 40:12–21.

Monoranu CM, Apfelbacher M, Grünblatt E, Puppe B, Alafuzoff I, Ferrer I, Al-Saraj S, Keyvani K, Schmitt A, Falkai P, Schittenhelm J, Halliday G, Kril J, Harper C, McLean C, Riederer P, Roggendorf W (2009) pH measurement as quality control on human post mortem brain tissue: a study of the BrainNet Europe consortium. Neuropathol Appl Neurobiol 35:329–337.

Patro R, Duggal G, Love MI, Irizarry RA, Kingsford C (2017) Salmon provides fast and bias: aware quantification of transcript expression. Nat Methods 14:417–419.

Quesnel-Vallières M, Dargaei Z, Irimia M, Gonatopoulos-Pournatzis T, Ip JY, Wu M, Sterne-Weiler T, Nakagawa S, Woodin MA, Blencowe BJ,

Cordes SP (2016) Misregulation of an activity-dependent splicing network as a common mechanism underlying autism spectrum disorders. Mol Cell 64:1023–1034.

Rusconi F, Battaglioli E (2018) Acute stress-induced epigenetic modulations and their potential protective role toward depression. Front Mol Neurosci 11:184.

Rusconi F, Mancinelli E, Colombo G, Cardani R, Da Riva L, Bongarzone I, Meola G, Zippel R (2010) Proteome profile in Myotonic Dystrophy type 2 myotubes reveals dysfunction in protein processing and mitochondrial pathways. Neurobiol Dis 38:273–280.

Rusconi F, Paganini L, Braida D, Ponzoni L, Toffolo E, Maroli A, Landsberger N, Bedogni F, Turco E, Pattini L, Altruda F, De Biasi S, Sala M, Battaglioli E (2015) LSD1 neurospecific alternative splicing controls neuronal excitability in mouse models of epilepsy. Cereb Cortex 25:2729–2740.

Rusconi F, Grillo B, Ponzoni L, Bassani S, Toffolo E, Paganini L, Mallei A, Braida D, Passafaro M, Popoli M, Sala M, Battaglioli E (2016) LSD1 modulates stress-evoked transcription of immediate early genes and emotional behavior. Proc Natl Acad Sci USA113:3651–3656.

Rusconi F, Grillo B, Toffolo E, Mattevi A, Battaglioli E (2017) NeuroLSD1: splicing-generated epigenetic enhancer of neuroplasticity. Trends Neurosci 40:28–38.

Rusconi F, Rubino T, Battaglioli E (2020) Endocannabinoid-epigenetic crosstalk: a bridge toward stress coping. Int J Mol Sci 21:6252.

Sengar AS, Li H, Zhang W, Leung C, Ramani AK, Saw NM, Wang Y, Tu Y, Ross PJ, Scherer SW, Ellis J, Brudno M, Jia Z, Salter MW (2019) Control of long-term synaptic potentiation and learning by alternative splicing of the NMDA receptor subunit GluN1. Cell Rep 29:4285–4294.e4285.

Spreafico M, Grillo B, Rusconi F, Battaglioli E, Venturin M (2018) Multiple layers of CDK5R1 regulation in Alzheimer's disease implicate long noncoding RNAs. Int J Mol Sci 19:2022.

Sullivan PF (2015) Genetics of disease: associations with depression. Nature 523:539–540.

Thalhammer A, Jaudon F, Cingolani LA (2020) Emerging roles of activity-dependent alternative splicing in homeostatic plasticity. Front Cell Neurosci 14:104.

Toffolo E, Rusconi F, Paganini L, Tortorici M, Pilotto S, Heise C, Verpelli C, Tedeschi G, Maffioli E, Sala C, Mattevi A, Battaglioli E (2014) Phosphorylation of neuronal Lysine-Specific Demethylase 1LSD1/KDM1A impairs transcriptional repression by regulating interaction with CoREST and histone deacetylases HDAC1/2. J Neurochem 128:603–616.

Trujillo CA, et al. (2021) Reintroduction of the archaic variant of NOVA1 in cortical organoids alters neurodevelopment. Science 371:eaax2537.

Turrigiano G (2012) Homeostatic synaptic plasticity: local and global mechanisms for stabilizing neuronal function. Cold Spring Harb Perspect Biol 4:a005736.

Wang J, Telese F, Tan Y, Li W, Jin C, He X, Basnet H, Ma Q, Merkurjev D, Zhu X, Liu Z, Zhang J, Ohgi K, Taylor H, White RR, Tazearslan C, Suh Y, Macfarlan TS, Pfaff SL, Rosenfeld MG (2015) LSD1n is an H4K20 demethylase regulating memory formation via transcriptional elongation control. Nat Neurosci 18:1256–1264.

Xu B, Roos JL, Levy S, van Rensburg EJ, Gogos JA, Karayiorgou M (2008) Strong association of de novo copy number mutations with sporadic schizophrenia. Nat Genet 40:880–885.

Zhang C, Zhang Z, Castle J, Sun S, Johnson J, Krainer AR, Zhang MQ (2008) Defining the regulatory network of the tissue-specific splicing factors Fox-1 and Fox-2. Genes Dev 22:2550–2563.

Zhang C, Frias MA, Mele A, Ruggiu M, Eom T, Marney CB, Wang H, Licatalosi DD, Fak JJ, Darnell RB (2010) Integrative modeling defines the Nova splicing-regulatory network and its combinatorial controls. Science 329:439–443.

Zibetti C, Adamo A, Binda C, Forneris F, Toffolo E, Verpelli C, Ginelli E, Mattevi A, Sala C, Battaglioli E (2010) Alternative splicing of the histone demethylase LSD1/KDM1 contributes to the modulation of neurite morphogenesis in the mammalian nervous system. J Neurosci 30:2521–2532.